

Photoinduced Interlayer Dynamics in T_d -MoTe₂: A Broadband Pump-Probe Study

Meixin Cheng^a, Shazhou Zhong^b, Nicolas Rivas^{a#}, Tina Dekker^b, Ariel Alcides Petruk^a, Patrick Gicala^a, Kostyantyn Pichugin^a, Fangchu Chen^b, Xuan Luo^c, Yuping Sun^{c,d,e}, Adam W. Tsen^b, Germán Sciaini^{a*}.

*Correspondence: gsciaini@uwaterloo.ca

[#]Present address: Nuclear Engineering Group, McMaster University, Hamilton, Ontario, L8S 4K1, Canada.

- ^a. The Ultrafast electron Imaging Lab, Department of Chemistry, and Waterloo Institute for Nanotechnology, University of Waterloo, Waterloo, Ontario N2L 3G1, Canada
- ^b. Institute for Quantum Computing, Department of Physics and Astronomy, Department of Electrical and Computer Engineering, and Department of Chemistry, University of Waterloo, Waterloo, Ontario N2L 3G1, Canada
- ^c. Key Laboratory of Materials Physics, Institute of Solid-State Physics, Chinese Academy of Sciences, Hefei 230031, People's Republic of China
- ^d. High Magnetic Field Laboratory, Chinese Academy of Sciences, Hefei, 230031, China
- ^e. Collaborative Innovation Center of Advanced Microstructures, Nanjing University, Nanjing, 210093, China

Abstract

We report on time-resolved broadband transient reflectivity (tr-bb-TR) measurements performed on a bulk single crystal of T_d -MoTe₂ as a function of the incident pump fluence (F). Tr-bb-TR data unveil photoinduced electronic changes progressing on the sub-picosecond timescale as well as the dynamics of the coherent low-frequency 1A_1 interlayer shear phonon. Our results indicate a gradual evolution of both the TR and the 1A_1 Fourier intensity spectra as a function of F , ruling out the threshold-like change that has been associated with the ultrafast photoinduced $T_d \rightarrow 1T'$ phase transition. We also observe a large redshift of the 1A_1 Fourier spectral features, which suggests that large renormalization effects are taking place on interband transitions that are dielectrically susceptible to the 1A_1 interlayer phonon displacement.

Keywords: Broadband spectroscopy, transient reflectivity, MoTe₂, Weyl semimetal, photoinduced phase transitions, carrier dynamics, phonon dynamics, intralayer effects, interlayer effects, transition metal dichalcogenides, 2D materials.

MoTe₂ is one of the few two-dimensional transition metal dichalcogenides (2D-TMDCs) that presents different polytypes with phase transitions that can be further controlled by temperature¹, alloying², strain³, electrostatic gating⁴, and dimensionality⁵. Relevant to the present work is the non-centrosymmetric T_d state⁶⁻⁸, which is purported to be a Weyl semimetallic phase⁶⁻⁸ and displays an orthorhombic unit cell with a c -axis inclination angle (α) of 90° with respect to the plane of the layer. Above a critical temperature of $T_c \approx 250$ K, T_d -MoTe₂ undergoes the displacement of adjacent Te-Mo-Te layers to transition to the centrosymmetric $1T'$ phase, that is characterized by a monoclinic unit cell with $\alpha = 93.92^\circ$. Both crystalline phases share a distorted intralayer structure in which the configuration of Mo centers surrounded by their neighboring Te atoms deviates substantially from the ideal octahedron of the trivial $1T$ state, presenting alternating shorter and longer Mo-Mo distances⁹, see Fig. 1(a).

Furthermore, inversion symmetry breaking below T_c results in the appearance of a characteristic low-frequency Raman-active interlayer shear phonon mode ($^1A_1 \approx 13$ cm⁻¹), see Fig. 1. This eminent $T_d \rightarrow 1T'$ phase-change signature and the possibility to control Weyl topologies through optical pumping of carriers have made the T_d phase an attractive candidate to explore the effects of femtosecond (fs) optical excitation¹⁰⁻¹⁵. Time- and angle-resolved photoelectron spectroscopy (tr-ARPES) revealed an enhanced relaxation rate of photoexcited electrons when compared to the $1T'$ phase¹⁰ as well as light induced band gap renormalization effects¹⁵. In a detailed investigation based on time-resolved single color transient reflectivity (tr-TR) and time-resolved second harmonic generation (tr-SHG) measurements, Zhang et al.^{11,12} reported the discovery of an ultrafast photoinduced $T_d \rightarrow 1T'$ phase transition that proceeds in only ~ 700 fs. Moreover, a very recent time-resolved ultrafast electron diffraction (tr-UED) study by Qi et al.¹⁴ provides evidence for the photoinduced suppression of the intralayer distortion in about 300 fs with a concomitant,

albeit small, intralayer displacement of only a few picometers (pm). The later observation is consistent with the small interlayer displacement of ~ 8 pm observed by tr-UED following intense THz field excitation of the analogous compound, T_d -WTe₂¹³. The use of SHG in the study of single- to multi-layer 2D-TMDCs^{16–20} has gained attraction owing to fact that the second order nonlinear susceptibility, $\chi^{(2)}$, vanishes in centrosymmetric systems. However, a discrepancy seems to exist between the conclusions drawn from the interpretation of structural data arising from tr-UED^{13,14} experiments and those attained via tr-SHG measurements^{11–13}. The latter appear to indicate the nearly disappearance of the non-centrosymmetric character of T_d -MTe₂ (M = Mo, W), and therefore a complete transformation to a $1T'$ -like phase. It should be noticed that, unlike most commonly employed nonlinear optical crystals, the $\chi^{(2)}$ of 2D-TMDCs has shown to be strongly dependent on strain^{16–19} and temperature^{11,12,20}, complicating the analysis of tr-SHG^{11–14} signals, and thus justifying this apparent controversy.

In this letter, we show fluence-dependent time-resolved broadband transient reflectivity (tr-bb-TR) measurements carried out in a bulk single crystal of T_d -MoTe₂ at a base temperature of $T = 77$ K, i.e., well below T_c as well as in the $1T'$ phase at room temperature, $T = 295$ K. Analyses of bb-TR and coherent 1A_1 Fourier intensity spectra as a function of the incident pump fluence (F) reveal a strong dependence on the probed photon energy (E_{probe}), deviations from the linear behaviour, as well as a progressive renormalization effect on electronic transitions that are susceptible to the coherent 1A_1 phonon displacement. Our results do not support the occurrence of the ultrafast photoinduced $T_d \rightarrow 1T'$ phase transition^{11,12}. Instead, they suggest the progressive development of photoinduced interlayer strain¹³ and/or the suppression of the intralayer distortion¹⁴, acting as a competing electron-phonon relaxation pathway with increasing F .

In our tr-spectroscopic experiments, ≈ 100 -fs pump pulses centered at a photon excitation energy of $E_{\text{exc}} = 1.2$ eV (wavelength of $\lambda = 1030$ nm) were implemented to drive the electron gas and the phonon bath out of equilibrium. Changes in the dielectric properties of the material arising from electronic population changes, hot-carrier energy relaxation processes, and coherent phonon oscillations were probed by time-delayed supercontinuum white light pulses with E_{probe} spanning from ≈ 1.3 eV to 2.3 eV. Measurements were conducted using a quasi-collinear arrangement with an angle of 10° between the incident pump and probe beams, which carried out crossed polarizations. The probe beam and pump beam spot sizes at the crystal's surface were approximately $50 \mu\text{m}$ and $400 \mu\text{m}$ fwhm (full width at half maximum), respectively. High-quality tr-bb-TR data allowed the observation of carrier and phonon dynamics at gradually increasing F . The incident pump fluence was varied through the combination of a half-wave plate and a calcite polarizer. The repetition rate of laser system was 6 kHz and bb-TR spectra were obtained by modulating the pump beam with a mechanical chopper at 500 Hz. We minimized the collection time to avoid sample drift and excessive exposure to pump pulses and confirmed reversible sampling conditions up to the maximum $F \approx 5 \text{ mJ}\cdot\text{cm}^{-2}$ presented in this work. $1T'$ -MoTe₂ crystals were grown in house following the recipe of Zeum et al.⁹, and characterized via Raman and transport measurements^{5,21}.

Figure 1 illustrates some characteristic results obtained at $F = 1.90 \text{ mJ}\cdot\text{cm}^{-2}$. The tr-bb-TR spectrum presented in Fig. 1(b) reveals several key features. The strong and long-period oscillation corresponds to the coherent 1A_1 interlayer phonon mode ($\approx 13 \text{ cm}^{-1}$), whereas the weaker ones arise from the 2A_1 ($\approx 77 \text{ cm}^{-1}$) and the 5A_1 ($\approx 164 \text{ cm}^{-1}$) vibrational coherences²². In addition, there are clear spectral weight shifts and broadening that develop on the sub-picosecond (sub-ps) timescale following photoexcitation and are highlighted by the dashed rectangle in Fig.1 (b). The

characteristic time for these spectral changes is in agreement with the 300-fs decay time observed for the suppression of the intralayer distortion¹⁴ as well as the electron-electron and electron-phonon energy relaxation rate constants determined by tr-angle-resolved photoelectron spectroscopy in T_d -MoTe₂¹⁰. Moreover, very efficient electron-phonon coupling constants have been observed in several other 2D-TMDCs^{23–27}.

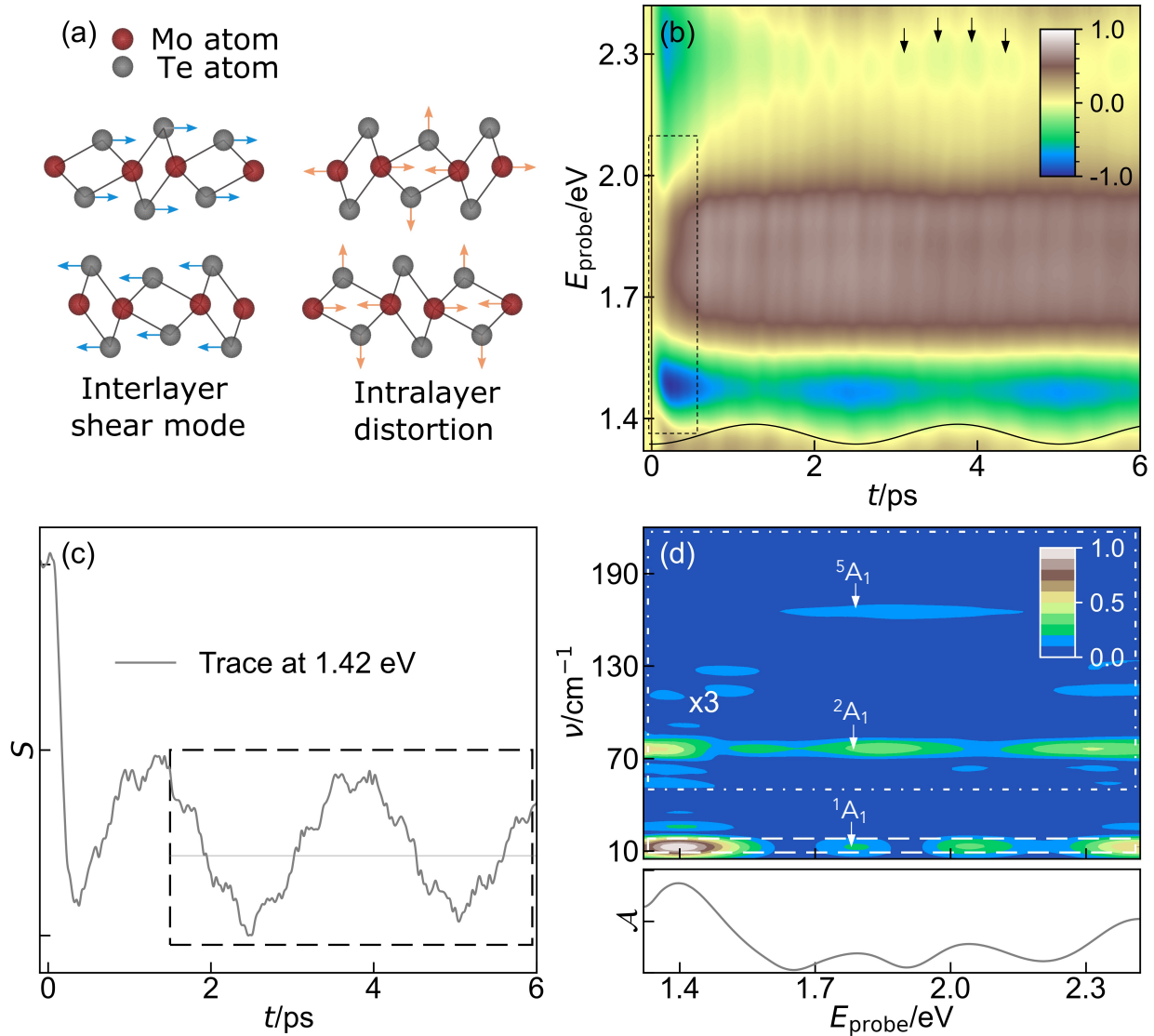


FIG. 1. Characteristic tr-bb-TR results obtained for T_d -MoTe₂ at 77 K and $F = 1.9 \text{ mJ}\cdot\text{cm}^{-2}$. (a) Illustration of the interlayer 1A_1 phonon mode (left) and the atomic displacements involved in the suppression of the

intralayer distortion (right). **(b)** Chirp-corrected tr-bb-TR spectrum. The vertical solid line indicates time zero. The sinusoidal trace and arrows were introduced to guide the eye. The former illustrates the spectral amplitude modulation introduced by the ${}^1A_1 \sim 13 \text{ cm}^{-1}$ phonon mode oscillation, which follows a cosine or dispersive type of coherent phonon excitation. The latter pinpoints the period of the ${}^2A_1 \sim 77 \text{ cm}^{-1}$ vibrational coherence. The dashed elongated rectangle highlights the observed spectral changes occurring at early times. **(c)** Temporal trace at $E_{\text{probe}} = 1.42 \text{ eV}$. The dashed rectangle indicates the portion of the trace employed to carry out further FFT analysis. **(d)** Fourier intensity map obtained from residuals as the one shown in panel **c**. The weaker FFT-amplitudes of the characteristic 2A_1 (77 cm^{-1}) and 5A_2 (164 cm^{-1}) phonons of the T_d phase are also shown with their intensities scaled by a factor of 3 as indicated by the dash-dotted rectangle.

Figure 1(c) shows a slice of the tr-bb-TR spectrum at $E_{\text{probe}} = 1.42 \text{ eV}$. This time-trace was fitted to remove the electronic background signal and generate a residual (inset) for further fast Fourier transform (FFT) analysis. We limited our evaluations to $t > +1.5 \text{ ps}$ to circumvent the observed initial spectral changes and enable the automated fitting routine of large data sets. At $t > +1.5 \text{ ps}$, electronic effects have reached a quasi-steady state, i.e., hot electrons have transferred most of their excess energy to the lattice via electron-electron and electron-phonon scattering processes within the conduction band. Therefore, time-dependent reflectivity changes at $t > +1.5 \text{ ps}$ are mostly governed by the oscillatory dynamics of coherently excited phonons. This procedure was applied at each value of E_{probe} , yielding the Fourier intensity map displayed in the top panel of Fig. 1(d). The bottom panel of Fig. 1(d) exhibits the values of the FFT-amplitude of the 1A_1 vibrational coherence (\mathcal{A}) as a function of E_{probe} , which were obtained through averaging along the small frequency interval specified by the dashed rectangle shown in the top panel of Fig. 1(d). We were able to determine the effects of increasing F on the TR spectrum (S), \mathcal{A} and the central frequency (ν_c) of the coherent 1A_1 phonon. These findings are summarized in Fig. 2.

Different theories have been put forward to explain the mechanism for the generation of coherent A_1 phonons in simple semimetals and semiconductors, asserting the challenges involved in describing the driving force responsible for launching such coherent nuclear motion^{28–37}. The sinusoidal curve in Fig. 1(b) pinpoints the phase of the 1A_1 vibrational coherence relative to time zero and indicates a cosine or displacive type of coherent phonon generation^{28,35}. Figures 2(a) and 2(b) display the changes of F -normalized spectra (S/F) spectra as a function of F for the T_d and $1T'$ phases, respectively. The bb-TR spectra were obtained by averaging data in the time domain between $t \approx +2.5$ ps and +5ps. This temporal interval corresponds approximately to one period of the 1A_1 phonon, see Fig. 1(c) and inset in Fig. 2(a), and this procedure was done to wash out the oscillatory effect caused by the 1A_1 and 2A_1 coherences on the TR signal. It is often expected for S to scale approximately proportionally with F , or in other words to remain constant when normalized by F . This is indeed the case for the optical response of the $1T'$ phase, which is illustrated in Fig. 2(b). In contrast, the dielectric response of the T_d state presents large deviations from linear behavior at $E_{\text{probe}} \approx 1.45$ eV. In addition, it is worth to mention that the TR spectra in Fig. 2(b) has been rescaled by a factor of 2 with respect to those shown in Fig. 2(a). These weaker TR signals can be explained by the higher baseline temperature of the $1T'$ phase, which leads to a higher population of thermal carriers, and therefore a relatively smaller change arising from the additionally photoexcited electron-hole pairs. The interpretation of the observed TR spectral changes is rather challenging since our E_{probe} range involves high-energy interband transitions³⁸.

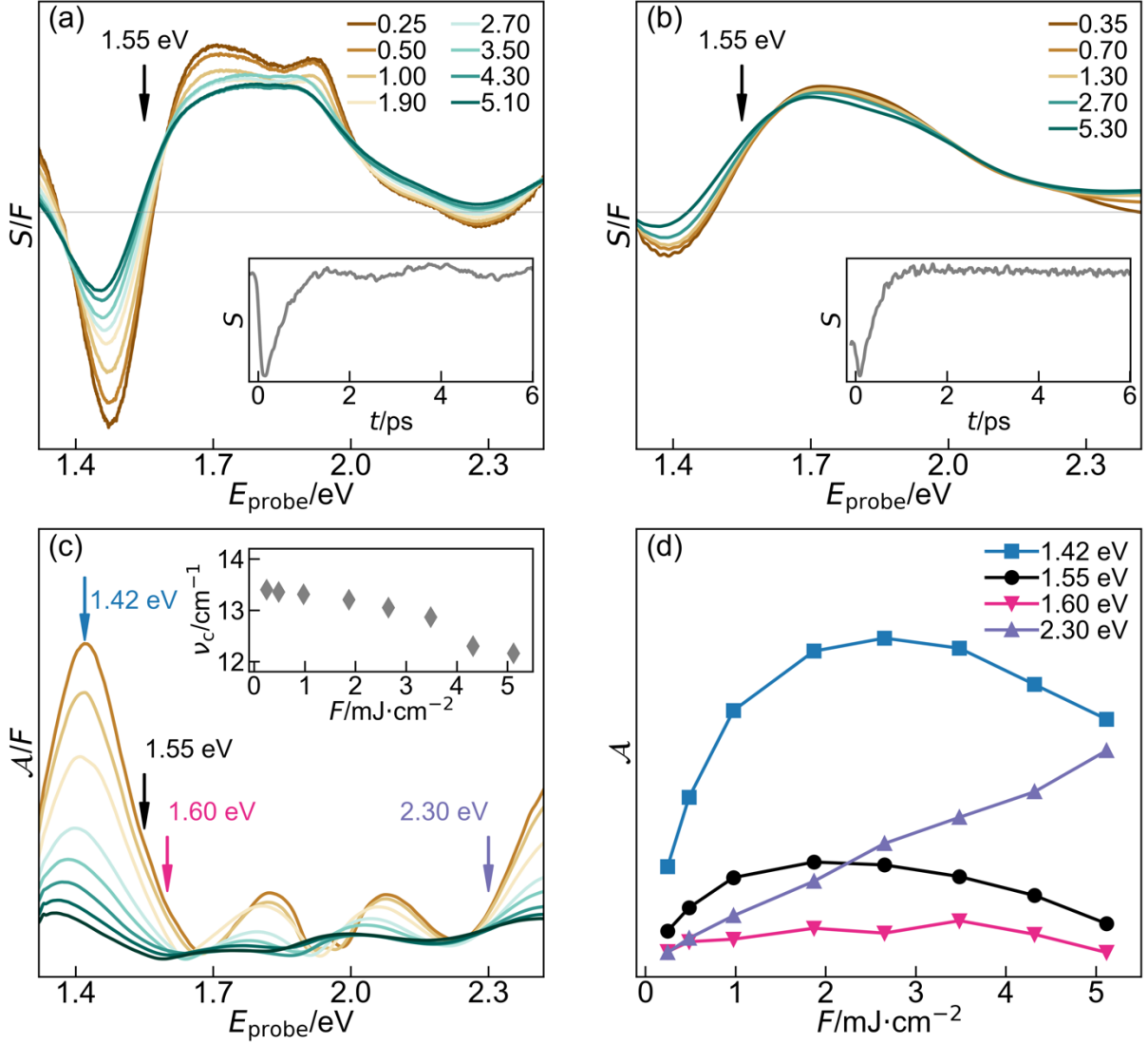


FIG. 2. (a), (b) Fluence-normalized transient spectra (S/F) for the T_d (a) and $1T'$ (b) phases. The traces were time-averaged between $t \approx 2.5$ ps - 5ps (one 1A_1 phonon period) to wash out the effect of the 1A_1 phonon oscillation in the T_d phase. The traces in panel **b** were scaled by a factor of 2. The insets show the characteristics temporal traces obtained at $E_{\text{probe}} = 1.55$ eV (arrows) and $F = 1.90$ $\text{mJ}\cdot\text{cm}^{-2}$ (a) and $F = 2.70$ $\text{mJ}\cdot\text{cm}^{-2}$ (b). (c) Fluence-normalized 1A_1 Fourier intensity spectra (\mathcal{A}/F). The inset shows the 1A_1 phonon frequency determined as a function of F . These were obtained via fitting of time traces at $E_{\text{probe}} \approx 1.4$ eV using a sine function. The arrows indicate the values of E_{probe} at which \mathcal{A} is plotted on panel (d). (d) Fluence dependence of \mathcal{A} at various E_{probe} .

Figure 2(c) exhibits the F -dependence of F -normalized 1A_1 Fourier intensity spectra (\mathcal{A}/F). The most noteworthy observation is the progressive redshift of \mathcal{A} with increasing F . This observation suggests that the interband transitions that are dielectrically susceptible to the coherent 1A_1 phonon displacement experience a large degree of renormalization and they are likely the cause for the deviations observed in S/F . Figure 2(d) shows the F -dependence of \mathcal{A} for some selected E_{probe} values. Our results at $E_{\text{probe}} = 1.55$ eV are in reasonable agreement with those obtained by Zhang et al.^{11,12}. However, our bb-data reveals no abrupt or threshold like behavior that could indicate the progression of a sub-ps photoinduced nonthermal $T_d \rightarrow 1T'$ phase transition¹². Note that a phase transformation is expected to lead to the sudden disappearance of vibrational coherences³⁹. As can be discerned by eye inspection of Fig. 3, there is a clear continuity of the amplitudes of the 1A_1 and 2A_1 coherent phonon modes even at $F = 5.1$ mJ·cm⁻². At this photoexcitation level and according to the energy balance, $\int_{77\text{K}}^{T_{l,m}} C(T) dT = \frac{F(1-R)M}{\rho\delta}$, the lattice should transiently reach a maximum temperature $T_{l,m} \approx 480$ K that is well above T_c (C is the heat capacity of T_d -MoTe₂⁴⁰, $\delta \approx 50$ nm is the optical penetration depth of the pump beam⁴¹, $M = 351.1$ g·mol⁻¹ and $\rho = 7.78$ g·cm⁻³, and $R \approx 0.40$ is the reflectivity at the crystal-vacuum interface³⁸). We assumed that the latent heat for the $T_d \rightarrow 1T'$ phase transition is smaller than or of the order of the one for the transformation between $2H$ and $1T'$ polytypes (360 cal·mol⁻¹)³. This represents a small fraction (≈ 0.1 mJ·cm⁻²) of the absorbed fluence (≈ 3.1 mJ·cm⁻²) and can be then neglected. Hence, we found no evidence for an ultrafast photoinduced $T_d \rightarrow 1T'$ phase transition, neither nonthermal¹² nor thermal. Therefore, the observed TR changes and phonon dynamics are characteristic of a hotter T_d phase.

Figure 3(a) also reveals that the overall decrease of \mathcal{A}/F shown in Fig. 2(c) is not due to thermally induced decoherence affecting the damping constant of the coherent 1A_1 phonon. Note that the amplitude of the 1A_1 coherence at $E_{\text{probe}} \approx 1.4$ eV remains approximately constant within $t = +1.5$ ps and $+6.0$ ps. The increase of F , however, is found to lead to changes of the interlayer shear potential as evidenced by the strong softening of the 1A_1 phonon mode, see inset of Fig. 2(c).

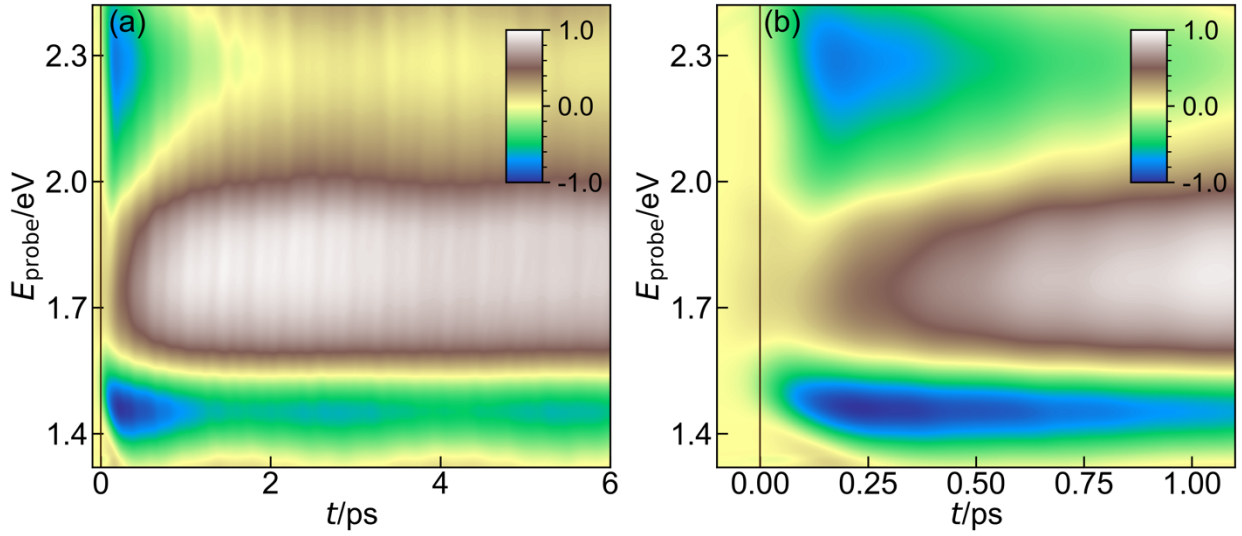


FIG. 3. (a) Chirp-corrected tr-bb-TR spectrum of T_d -MoTe $_2$ recorded at $T = 77$ K and $F = 5.1$ mJ-cm $^{-2}$. (b) Close-up view of the first picosecond following photoexcitation highlighting the smooth continuity of 1A_1 and 2A_1 coherences.

The success of known reversible ultrafast photoinduced phase transformations^{24,39,42–50} rests on the ability of the sample to return to its original ground-state configuration before the next pair of pump and probe pulses excite and interrogate the system again. We would like to emphasize that the actual atomic rearrangements in crystalline systems capable of withstanding billions of photoexcitation cycles are well localized within the frame of an arbitrary unit cell. In contrast, the $T_d \rightarrow 1T'$ phase transition comprises the relative displacement of adjacent Te-Mo-Te layers. This

process concerns many rigidly connected atoms that must respond collectively over the extent of a microscopic domain, and therefore it is unlikely to complete on the sub-ps timescale. Such a barrierless picture does not account for local variations in energy barriers and the degree of electronic delocalization. In fact, we believe that photoexcitation leads to a transiently hot T_d state that dissipates the excess of energy into the bulk before having sufficient time to structurally transition to the $1T'$ phase.

Our results agree with the scenario of the photoinduced formation of a strained hot T_d state with weaker cohesive interlayer forces, in which the suppression of the intralayer distortion¹⁴, i.e. a localized atomic rearrangement, and the presence of domain walls in the a - b plane and along the stacking c -axis⁵¹ may progressively facilitate a small shear displacement^{13,14}. Photoinduced phase transitions are playing an increasingly important role in quantum materials and devices designed to confer properties on demand⁵². We hope that our discussion will bring a better understanding of the requirements for structural phenomena to be able to proceed on ultrafast time scales.

Acknowledgements

We would like to thank Prof. Roberto Merlin (U. Michigan) and Dr. Ralph Ernstorfer (Fritz Haber Institute) for fruitful discussions and Prof. David Cory (U. Waterloo) for lending us the Oxford cryostat utilized in this work. G.S. acknowledge the support of the National Research Council of Canada, the Canada Foundation for Innovation, and Canada Research Chair program. A.W.T. acknowledges support from the US Army Research Office (W911NF-21-2-0136), Ontario Early Researcher Award (ER17-13-199), and the National Science and Engineering Research Council of Canada (RGPIN-2017-03815). This research was undertaken thanks in part to funding from the Canada First Research Excellence Fund. F.C., X. L. and Y.S. thank the support of the National

Key Research and Development Program under contracts 2016YFA0300404 and the National Nature Science Foundation of China under contracts 11674326, 11874357 and the Joint Funds of the National Natural Science Foundation of China and the Chinese Academy of Sciences' Large-Scale Scientific Facility under contracts U1832141 and U1932217.

Data availability

The data that support the findings of this study are available from the corresponding author upon reasonable request.

References

- ¹ M.B. Vellinga, R. de Jonge, and C. Haas, *J. Solid State Chem.* **2**, 299 (1970).
- ² D. Rhodes, D.A. Chenet, B.E. Janicek, C. Nyby, Y. Lin, W. Jin, D. Edelberg, E. Mannebach, N. Finney, A. Antony, T. Schiros, T. Klarr, A. Mazzoni, M. Chin, Y. -c Chiu, W. Zheng, Q.R. Zhang, F. Ernst, J.I. Dadap, X. Tong, J. Ma, R. Lou, S. Wang, T. Qian, H. Ding, R.M. Osgood, D.W. Paley, A.M. Lindenberg, P.Y. Huang, A.N. Pasupathy, M. Dubey, J. Hone, and L. Balicas, *Nano Lett.* **17**, 1616 (2017).
- ³ S. Song, D.H. Keum, S. Cho, D. Perello, Y. Kim, and Y.H. Lee, *Nano Lett.* **16**, 188 (2016).
- ⁴ L. Wang, I. Meric, P.Y. Huang, Q. Gao, Y. Gao, H. Tran, T. Taniguchi, K. Watanabe, L.M. Campos, D.A. Muller, J. Guo, P. Kim, J. Hone, K.L. Shepard, and C.R. Dean, *Science* **342**, 614 (2013).
- ⁵ R. He, S. Zhong, H.H. Kim, G. Ye, Z. Ye, L. Winford, D. McHaffie, I. Rilak, F. Chen, X. Luo, Y. Sun, and A.W. Tsen, *Phys. Rev. B* **97**, 041410 (2018).
- ⁶ A.A. Soluyanov, D. Gresch, Z. Wang, Q. Wu, M. Troyer, X. Dai, and B.A. Bernevig, *Nature* **527**, 495 (2015).
- ⁷ J. Jiang, Z.K. Liu, Y. Sun, H.F. Yang, C.R. Rajamathi, Y.P. Qi, L.X. Yang, C. Chen, H. Peng, C.-C. Hwang, S.Z. Sun, S.-K. Mo, I. Vobornik, J. Fujii, S.S.P. Parkin, C. Felser, B.H. Yan, and Y.L. Chen, *Nat. Commun.* **8**, 13973 (2017).
- ⁸ B. Yan and C. Felser, *Annu. Rev. Condens. Matter Phys.* **8**, 337 (2017).
- ⁹ D.H. Keum, S. Cho, J.H. Kim, D.-H. Choe, H.-J. Sung, M. Kan, H. Kang, J.-Y. Hwang, S.W. Kim, H. Yang, K.J. Chang, and Y.H. Lee, *Nat. Phys.* **11**, 482 (2015).
- ¹⁰ A. Crepaldi, G. Autès, G. Gatti, S. Roth, A. Sterzi, G. Manzoni, M. Zacchigna, C. Cacho, R.T. Chapman, E. Springate, E.A. Seddon, Ph. Bugnon, A. Magrez, H. Berger, I. Vobornik, M. Kalläne, A. Quer, K. Rossnagel, F. Parmigiani, O.V. Yazyev, and M. Grioni, *Phys. Rev. B* **96**, 241408 (2017).
- ¹¹ M.Y. Zhang, Z.X. Wang, Y.N. Li, L.Y. Shi, D. Wu, T. Lin, S.J. Zhang, Y.Q. Liu, C.N. Wang, Q.M. Liu, J. Wang, T. Dong, and N.L. Wang, *ArXiv180609075 Cond-Mat* (2018).

- ¹² M.Y. Zhang, Z.X. Wang, Y.N. Li, L.Y. Shi, D. Wu, T. Lin, S.J. Zhang, Y.Q. Liu, Q.M. Liu, J. Wang, T. Dong, and N.L. Wang, *Phys. Rev. X* **9**, 021036 (2019).
- ¹³ E.J. Sie, C.M. Nyby, C.D. Pemmaraju, S.J. Park, X. Shen, J. Yang, M.C. Hoffmann, B.K. Ofori-Okai, R. Li, A.H. Reid, S. Weathersby, E. Mannebach, N. Finney, D. Rhodes, D. Chenet, A. Antony, L. Balicas, J. Hone, T.P. Devereaux, T.F. Heinz, X. Wang, and A.M. Lindenberg, *Nature* **565**, 61 (2019).
- ¹⁴ Y. Qi, M. Guan, D. Zahn, T. Vasileiadis, H. Seiler, Y.W. Windsor, H. Zhao, S. Meng, and R. Ernstorfer, *ArXiv210514175 Cond-Mat* (2021).
- ¹⁵ S. Beaulieu, S. Dong, N. Tancogne-Dejean, M. Dendzik, T. Pincelli, J. Maklar, R.P. Xian, M.A. Sentef, M. Wolf, A. Rubio, L. Rettig, and R. Ernstorfer, *Sci. Adv.* **7**, eabd9275 (2021).
- ¹⁶ D. Li, C. Wei, J. Song, X. Huang, F. Wang, K. Liu, W. Xiong, X. Hong, B. Cui, A. Feng, L. Jiang, and Y. Lu, *Nano Lett.* **19**, 4195 (2019).
- ¹⁷ J. Liang, J. Zhang, Z. Li, H. Hong, J. Wang, Z. Zhang, X. Zhou, R. Qiao, J. Xu, P. Gao, Z. Liu, Z. Liu, Z. Sun, S. Meng, K. Liu, and D. Yu, *Nano Lett.* **17**, 7539 (2017).
- ¹⁸ L. Mennel, M. Paur, and T. Mueller, *APL Photonics* **4**, 034404 (2018).
- ¹⁹ L. Zhou, H. Fu, T. Lv, C. Wang, H. Gao, D. Li, L. Deng, and W. Xiong, *Nanomaterials* **10**, 2263 (2020).
- ²⁰ A.R. Khan, B. Liu, L. Zhang, Y. Zhu, X. He, L. Zhang, T. Lü, and Y. Lu, *Adv. Opt. Mater.* **8**, 2000441 (2020).
- ²¹ S. Zhong, A. Tiwari, G. Nichols, F. Chen, X. Luo, Y. Sun, and A.W. Tsien, *Phys. Rev. B* **97**, 241409 (2018).
- ²² K. Zhang, C. Bao, Q. Gu, X. Ren, H. Zhang, K. Deng, Y. Wu, Y. Li, J. Feng, and S. Zhou, *Nat. Commun.* **7**, 13552 (2016).
- ²³ L. Perfetti, P.A. Loukakos, M. Lisowski, U. Bovensiepen, H. Berger, S. Biermann, P.S. Cornaglia, A. Georges, and M. Wolf, *Phys. Rev. Lett.* **97**, 067402 (2006).
- ²⁴ M. Eichberger, H. Schäfer, M. Krumova, M. Beyer, J. Demsar, H. Berger, G. Moriena, G. Sciaini, and R.J.D. Miller, *Nature* **468**, 799 (2010).
- ²⁵ Y.M. Dai, J. Bowlan, H. Li, H. Miao, S.F. Wu, W.D. Kong, P. Richard, Y.G. Shi, S.A. Trugman, J.-X. Zhu, H. Ding, A.J. Taylor, D.A. Yarotski, and R.P. Prasankumar, *Phys. Rev. B* **92**, 161104 (2015).
- ²⁶ L. Waldecker, R. Bertoni, H. Hübener, T. Brumme, T. Vasileiadis, D. Zahn, A. Rubio, and R. Ernstorfer, *Phys. Rev. Lett.* **119**, 036803 (2017).
- ²⁷ K. Rossnagel, *J. Phys. Condens. Matter* **23**, 213001 (2011).
- ²⁸ H.J. Zeiger, J. Vidal, T.K. Cheng, E.P. Ippen, G. Dresselhaus, and M.S. Dresselhaus, *Phys. Rev. B* **45**, 768 (1992).
- ²⁹ R. Scholz, T. Pfeifer, and H. Kurz, *Phys. Rev. B* **47**, 16229 (1993).
- ³⁰ A.V. Kuznetsov and C.J. Stanton, *Phys. Rev. Lett.* **73**, 3243 (1994).
- ³¹ L. Dhar, J.A. Rogers, and K.A. Nelson, *Chem. Rev.* **94**, 157 (1994).
- ³² G.A. Garrett, T.F. Albrecht, J.F. Whitaker, and R. Merlin, *Phys. Rev. Lett.* **77**, 3661 (1996).
- ³³ R. Merlin, *Solid State Commun.* **102**, 207 (1997).
- ³⁴ M.F. DeCamp, D.A. Reis, P.H. Bucksbaum, and R. Merlin, *Phys. Rev. B* **64**, 092301 (2001).
- ³⁵ T.E. Stevens, J. Kuhl, and R. Merlin, *Phys. Rev. B* **65**, 144304 (2002).

- ³⁶ O.V. Misochko, M. Hase, and M. Kitajima, *Phys. Solid State* **46**, 1741 (2004).
- ³⁷ D.M. Riffe and A.J. Sabbah, *Phys. Rev. B* **76**, 085207 (2007).
- ³⁸ D. Santos-Cottin, E. Martino, F. Le Mardelé, C. Witteveen, F.O. von Rohr, C.C. Homes, Z. Rukelj, and A. Akrap, *Phys. Rev. Mater.* **4**, 021201 (2020).
- ³⁹ S. Wall, D. Wegkamp, L. Foglia, K. Appavoo, J. Nag, R.F. Haglund Jr, J. Stähler, and M. Wolf, *Nat. Commun.* **3**, 721 (2012).
- ⁴⁰ H.L. Kiwia and E.F. Westrum Jr, *J. Chem. Thermodyn.* **7**, 683 (1975).
- ⁴¹ A.R. Beal, J.C. Knights, and W.Y. Liang, *J. Phys. C Solid State Phys.* **5**, 3540 (1972).
- ⁴² A. Cavalleri, Cs. Tóth, C.W. Siders, J.A. Squier, F. Ráksi, P. Forget, and J.C. Kieffer, *Phys. Rev. Lett.* **87**, 237401 (2001).
- ⁴³ A. Cavalleri, Th. Dekorsy, H.H.W. Chong, J.C. Kieffer, and R.W. Schoenlein, *Phys. Rev. B* **70**, 161102 (2004).
- ⁴⁴ P. Baum, D.-S. Yang, and A.H. Zewail, *Science* **318**, 788 (2007).
- ⁴⁵ Z. Tao, T.-R.T. Han, S.D. Mahanti, P.M. Duxbury, F. Yuan, C.-Y. Ruan, K. Wang, and J. Wu, *Phys. Rev. Lett.* **109**, 166406 (2012).
- ⁴⁶ V.R. Morrison, R.P. Chatelain, K.L. Tiwari, A. Hendaoui, A. Bruhács, M. Chaker, and B.J. Siwick, *Science* **346**, 445 (2014).
- ⁴⁷ S. Wall, S. Yang, L. Vidas, M. Chollet, J.M. Glowia, M. Kozina, T. Katayama, T. Henighan, M. Jiang, T.A. Miller, D.A. Reis, L.A. Boatner, O. Delaire, and M. Trigo, *Science* **362**, 572 (2018).
- ⁴⁸ M. Chollet, L. Guerin, N. Uchida, S. Fukaya, H. Shimoda, T. Ishikawa, K. Matsuda, T. Hasegawa, A. Ota, H. Yamochi, G. Saito, R. Tazaki, S. Adachi, and S. Koshihara, *Science* **307**, 86 (2005).
- ⁴⁹ K. Onda, S. Ogihara, K. Yonemitsu, N. Maeshima, T. Ishikawa, Y. Okimoto, X. Shao, Y. Nakano, H. Yamochi, G. Saito, and S. Koshihara, *Phys. Rev. Lett.* **101**, 067403 (2008).
- ⁵⁰ M. Gao, C. Lu, H. Jean-Ruel, L.C. Liu, A. Marx, K. Onda, S. Koshihara, Y. Nakano, X. Shao, T. Hiramatsu, G. Saito, H. Yamochi, R.R. Cooney, G. Moriena, G. Sciaini, and R.J.D. Miller, *Nature* **496**, 343 (2013).
- ⁵¹ F.-T. Huang, S. Joon Lim, S. Singh, J. Kim, L. Zhang, J.-W. Kim, M.-W. Chu, K.M. Rabe, D. Vanderbilt, and S.-W. Cheong, *Nat. Commun.* **10**, 4211 (2019).
- ⁵² D.N. Basov, R.D. Averitt, and D. Hsieh, *Nat. Mater.* **16**, 1077 (2017).